Sympathetic neuron derived NPY protects from obesity by sustaining the mural progenitors of thermogenic adipocytes.

Yitao Zhu[1], Lu Yao[1], Ana Luisa Gallo-Ferraz[9], Bruna Bombassaro[9], Marcela R. Simoes[9], Ichitaro Abe[5, 10], Jing Chen[8], Gitalee Sarker[1], Alessandro Ciccarelli[4], Linna Zhou[11], Carl Lee[3], Noelia Martinez-Sanchez[2], Michael Dustin[3], Kurt Anderson[4], Cheng Zhan[7], Tamas Horvath[6], Licio A. Velloso[9], Shingo Kajimura[5], Ana I. Domingos[1]*

Author affiliation

[1]Department of Physiology, Anatomy and Genetics, University of Oxford, Oxford, OX3 1PT, UK

[2]Oxford Centre for Diabetes, Endocrinology and Metabolism Radcliffe Department of Medicine, University of Oxford, Oxford, OX3 9DU, UK

[3]Kennedy Institute of Rheumatology, University of Oxford, Oxford, OX3 7FY, UK

[4]Advanced Light Microscopy, The Francis Crick Institute, 1 Midland Road, London NW1 1AT, UK.

[5]Beth Israel Deaconess Medical Center, Division of Endocrinology, Diabetes & Metabolism, Harvard Medical School, Boston, MA, USA

[6]Department of Obstetrics/Gynecology and Reproductive Sciences, Yale University School of Medicine, New Haven 06520, CT, USA

[7]Department of Hematology, Division of Life Sciences and Medicine, University of Science and Technology of China, Hefei 230026, China.

[8]School of Sport Science, Beijing Sport University, Beijing 100084, China.

[9]Laboratory of Cell Signaling, Obesity and Comorbidities Research Center, University of Campinas, Brazil.

[10]Department of Cardiology and Clinical Examination, Oita University, Faculty of Medicine, Oita, Japan.

[11]Ludwig Institute for Cancer Research Ltd, University of Oxford, Nuffield Department of Medicine, Old Road Campus Research Building, Roosevelt Drive, Oxford OX3 7DQ, UK

Correspondence to Ana I. Domingos.
Department of Physiology, Anatomy and Genetics
University of Oxford
Oxford, OX3 1PT
ana.domingos@dpag.ox.ac.uk

Neuropeptide Y (NPY) is secreted by sympathetic nerves[1,2], but its direct impact on thermogenic adipocytes is unknown. Here we uncover the mechanism by which peripheral NPY protects from obesity. Our imaging of cleared murine brown and white adipose tissue (BAT and WAT) established that NPY$^+$ sympathetic axons are only a minority that mostly maps to the peri-vasculature; our analysis of single-cell RNA-sequencing datasets identifies mural cells as the main NPY-responsive cells in adipose tissues. We show that NPY sustains mural cells, which are known to be a source of beige cells in both BAT and WAT[3-5] and that NPY facilitates the differentiation to thermogenic adipocytes. We found that diet-induced obesity leads to neuropathy of NPY$^+$ axons and concomitant depletion of the mural cell pool of beige fat progenitors. This defect is replicated in conditional knockout (cKO) mice with NPY specifically abrogated from sympathetic neurons. These cKO mice have whitened iBAT with reduced thermogenic ability and lower energy expenditure even before the onset of obesity; they develop adult-onset obesity on a regular chow diet and are more susceptible to diet-induced obesity without increasing food consumption. Our results indicate that relative to central NPY, peripheral NPY produced by the sympathetic nerves has the opposite effect on body weight homeostasis by sustaining the proliferation of the mural cell progenitors of thermogenic adipocytes.

Main Text

Sympathetic nerves within both brown and white adipose tissue (BAT and WAT) locally release norepinephrine (NE) to directly induce lipolysis and thermogenesis[6,7]. NPY is co-released with NE[8], but the extent of NPY-releasing sympathetic nerves and their role in adipose tissue is not clear. Although many reports indicate that NPY in the brain stimulates appetite[9,10], knocking out NPY has no effect on daily food consumption[11,12], and mice without NPY receptors develop late-onset obesity despite eating less[13-15]. In humans, mutations in NPY have been linked to high body mass index (BMI) but not an unhealthy dietary pattern (https://hugeamp.org/gene.html?gene=NPY)[16]. These findings suggest that NPY from the central and sympathetic systems have contrasting impacts on maintaining body weight homeostasis. To test this hypothesis, we employed improved animal models in which NPY was selectively removed from sympathetic neurons, while leaving it intact in the brain.

1. In white and brown adipose tissues, NPY is exclusively sourced by one-third of TH$^+$ (Tyrosine Hydroxylase-positive) sympathetic axons that preferentially innervate the vasculature.

The published single-cell RNA-sequencing (scRNA-Seq) dataset of sympathetic ganglia[17] uncovers that only two out of five clusters of sympathetic neurons express an elevated level of NPY (Supplementary Figure 1a-c). The proportion of NPY^+ sympathetic neurons, which is about 40%, was verified by immunofluorescent co-staining of NPY and the sympathetic neuron marker tyrosine hydroxylase (TH) on superior cervical ganglia (SCG) and stellate ganglia (SG) (Supplementary Figure 1d-f). Similar TH/NPY overlap is observed on sympathetic axon bundles dissected from the inguinal adipose tissue (iWAT) (Figure 1a). We also observed that in the iWAT, NPY^+ axons are associated with the vasculature and form plexus around the vessels (Figure 1b). To determine the distribution of TH^+ and NPY^+ axons in the whole adipose tissue, we performed tissue clearing of the iWAT[18] and immunolabelled for TH, NPY and CD31, the latter of which marks the vascular endothelium. We confirmed that NPY^+ axons are a subgroup of sympathetic axons (Figure 1c&d). By quantifying the images as in Figure 1d, we found that the double positive TH^+NPY^+ axons make up 32.4% of all labelled axons; 59.3% of axons are TH^+NPY^- (Figure 1e-f). The images also indicate that NPY^+ axons preferentially innervate $CD31^+$ endothelium, and we confirmed that the percentage of NPY^+ axons overlapping with $CD31^+$ endothelium is higher than TH^+ axons by quantifying images as in Figure 1d (Figure 1g). Consistent with iWAT, we observed in intrascapular BAT (iBAT) that NPY^+ axons mainly innervate the vasculature (Figure 1h). To further determine which vessel branches are innervated by NPY^+ axons, we quantified light-sheet images (Supplementary Figure 2a) and found that the density of NPY^+ axons is the highest in 5th order branches (Supplementary Figure 2c-d), while NPY^+ axons do not innervate the 8th order branches (Supplementary Figure 2b-d). To determine if arteries or veins are innervated by NPY^+ axons in adipose tissue, we co-stained iWAT for NPY and EPHB4, a marker for veins[19], or SOX17, a marker for arteries[20]. The IF images indicate that no NPY^+ axons innervate $EPHB4^+$ vessels, while they innervate $SOX17^+$ vessels (Supplementary Figure 2e-f). Based on these observations, we conclude that NPY^+ sympathetic axons in adipose tissue preferentially innervate arterioles but not veins nor venules.

Moreover, it is worth noting that our NPY stains are exclusively axonal. Even though earlier studies proposed that adipose-tissue macrophages (ATM) can express *Npy*[21], this is negated by two scRNA-Seq datasets of the stromal-vascular fraction (SVF) of murine iWAT and iBAT[4,22] (Supplementary Figure 3a-d). Consistently, by using qPCR, we did not detect expression of *Npy* in sorted ATMs from $Cx3cr1^{GFP/+}$ reporter mice, despite the positivity of the *Adgre1* (F4/80) control (Supplementary Figure 3e-f).

2. The post-synaptic targets of NPY$^+$ sympathetic neurons in iWAT and iBAT are NPY1R$^+$ mural cells, which are progenitors of thermogenic adipocytes.

We then questioned what type of perivascular cells are the postsynaptic targets of NPY$^+$ axons in adipose tissues. By reanalysing the scRNA-Seq dataset of iWAT[22] and iBAT[4], we found *Npy1r* is highly expressed in mural cells that are marked by *Des*, *Myh11*, *Acta2* (αSMA), *Tagln*, *Cspg4* (NG2), and *Pdgfrb*, and NPY1R is a *bona fide* marker of mural cells within iWAT and iBAT (Figure 2a-d; Supplementary Figure 3a-b). To validate the scRNA-Seq datasets by qPCR, we sorted mural cells (live, CD31$^-$/CD45$^-$/PDGFRα$^-$/NG2$^+$ cells) and immune cells (live, CD31$^-$/CD45$^+$ cells) from the SVF of iWAT and iBAT (Supplementary Figure 3g) and did qPCR. Using this method, we independently confirmed that *Npy1r* and *Des* are highly expressed in mural cells but not in immune cells (Figure 2e). To confirm the existence of NPY1R in mural cells at the protein level, we dissected capillaries from adipose tissue and stained them with anti-CD31 and anti-NPY1R. We detected an NPY1R$^+$ cell wrapping the capillary (Figure 2f), whose morphology matches that of mural cells of fine capillaries, which are conventionally named as pericytes[23]. To confirm the colocalization of NPY1R with multiple mural cell marker observed in scRNA-Seq datasets (Supplementary Figure 4a), we immunolabelled vessel-containing samples dissected from adipose tissues of Npy1r^{Cre}; Rosa26^{tdTomato} mice for multiple mural cell markers including DES, αSMA, and NG2, and the images indicate that DES$^+$, αSMA$^+$, or NG2$^+$ mural cells are all labelled with NPY1R-tdTomato (Figure 2g, Supplementary Figure 4b-e). Based on the observations above, we demonstrate that mural cells are the target of NPY$^+$ axons and that they are NPY1R$^+$.

It is worth noticing that earlier reports of *Npy2r* and *Npy5r* expression by immune cells, preadipocytes and adipocytes[24-27] are negated by our analysis of the two scRNA-Seq datasets of both iBAT and iWAT, where *Npy5r* is undetectable, and *Npy2r* expression is only detectable in iWAT but negligible (Supplementary Figure 5a-b). Also, some previous reports of *Npy1r* expression[28] by adipocytes or macrophages are negated by a single-nucleus atlas of mouse white adipose tissue and a scRNA-Seq dataset of iBAT[4,29] as well as our qPCR result of sorted ATMs (Supplementary Figure 3f). Therefore, other than mural cells, no immune cells or adipocytes are likely to be the postsynaptic targets of NPY$^+$ axons in adipose tissue.

Mural cells can give rise to thermogenic adipocytes[3-5], and previously identified progenitors of beige cells (Lin$^-$/CD81$^+$) express *Npy1r* and mural cell markers[5] (Supplementary Figure 6a-c), which is further proven via our analysis of iWAT scRNA-Seq data (Supplementary Figure 6d). We confirmed that mural cells from both iWAT and iBAT are progenitors of thermogenic adipocytes by isolating and differentiating them *in vitro*[30] (Supplementary Figure 7a-b), and found they are more potent in differentiating into

thermogenic adipocytes than SVF (Supplementary Figure 7c-f). To demonstrate that NPY1R^{+} mural cells are progenitors of thermogenic adipocytes under physiological conditions, we immunolabelled iBAT of Npy1r^{Cre}; Rosa26^{tdTomato} room-temperature (RT) -housed mice for UCP1; using this lineage-tracing approach, we observe that both mural cells and a subgroup of UCP1^{+} adipocytes are co-labelled with NPY1R-tdTomato (Figure 2h-i). Since adipocytes do not express *Npy1r* (Figure 2c), we reason that these NPY1R-tdTomato^{+}UCP1^{+} thermogenic adipocytes are lineage-traced to NPY1R^{+} mural cells. It is worth noticing that NPY1R-tdTomato only labels multi-locular UCP1^{+} adipocytes in iBAT and iWAT, but not UCP1^{-} unilocular white adipocytes (Supplementary Figure 8a-c), which indicates that NPY1R is specifically expressed in the progenitor of thermogenic adipocytes. Based on the observations above and published literature[3-5], we conclude that NPY1R^{+} mural cells are progenitors of thermogenic adipocytes.

3. NPY promotes mural cell proliferation, facilitates the neogenesis of thermogenic adipocytes, and sustains their ability to differentiate into thermogenic adipocytes.

NPY1R is a kind of G protein-coupled receptor (GPCR) that can activate MAPK pathways after binding to NPY, and the phosphorylated MAPK downstream of NPY1R is ERK[31-33]. Since MAPK pathway is a canonical regulator of cell proliferation[34], we then questioned if NPY can promote the proliferation of mural cells. By isolating mural cells and adding NPY, we observed that NPY promotes the proliferation of both iWAT and iBAT mural cells (Figure 3a-e). We further observed that PD98059, which is a ERK inhibitor, blocked NPY mitogenic effect (Supplementary Figure 9a-b), which indicates that NPY promotes the proliferation of mural cells via ERK. Consistent with this, we found that NPY increased the proportion of αSMA^{+} mural cells in cultured SVF and CD81^{+} cells (Supplementary Figure 10a-c). Since mural cells are proven to be the progenitors of thermogenic adipocytes (Supplementary Figure 7c-f), we reasoned that NPY could facilitate the neogenesis of thermogenic adipocytes (Supplementary Figure 10d). To directly prove this, we differentiated iWAT SVF and progenitors of thermogenic adipocytes isolated from iWAT and iBAT and found that NPY facilitates the differentiation into thermogenic adipocytes by upregulating thermogenic genes without affecting adipogenic genes (Supplementary Figure 11a-d&f-g). Also, NPY increased the maximal respiratory capacity of adipocytes differentiated from iWAT beige adipocyte progenitors (Supplementary Figure 11e). We further demonstrated that NPY does not affect adipogenesis using NPY1R^{+} 3T3-L1 cells (Supplementary Figure 12c-d), so the effect of NPY is specific to the differentiation of thermogenic adipocytes. Previous reports have demonstrated that mural cells can be regulated by PDGF-B[35]. On one hand, it is a factor required for the recruitment of mural

cells; on the other hand, elevated levels of PDGF-B can decrease mural cells both *in vitro* and *in vivo* by upregulating fibroblast markers and promoting the proliferation of fibroblasts[36,37]. We then questioned whether NPY can sustain mural cells when being challenged with PDGF-B. This is physiologically relevant since diet-induced-obesity (DIO) increases PDGF-B in adipose tissue[37]. By treating isolated mural cells with PDGF-BB, we found that PDGF-BB indeed decreased the proportion of mural cells and increased the number of spindle-shaped PDGFRα$^+$ fibroblasts, an effect that is counteracted by NPY (Supplementary Figure 13a-b). Furthermore, using qPCR, we demonstrate that NPY can restore the expression of *Npy1r* and other mural cell markers including *Pdgfrb*, *Rgs5*, and *Angpt1* that are downregulated by PDGF-BB (Supplementary Figure 13c-e). Since mural cells have been identified as the progenitor of thermogenic adipocytes, we then examined whether NPY can preserve their beiging ability against PDGF-BB. We observe that PDGF-BB-treatment downregulates thermogenic and adipogenic genes, while NPY can restore their expression (Supplementary Figure 13f-h). Based on the observations above, we demonstrate *in vitro* that NPY can sustain mural cells as the progenitors of thermogenic adipocytes

4. High-fat diet-induced obesity depletes NPY+ innervation and mural cells in adipose tissue, increasing vascular leakiness.

To test whether NPY$^+$ sympathetic axons are also affected by the obesity-induced sympathetic neuropathy in the adipose tissue[38], we immunolabelled the cleared iWAT of normal diet (ND)- and high-fat diet (HFD)-treated mice for NPY and CD31. Our light-sheet images show that the density of NPY$^+$ axons is significantly decreased in the iWAT of HFD-treated mice compared with ND-treated lean mice and, as a result, the percentage of vessels innervated by NPY$^+$ axons is significantly decreased as well (Supplementary Figure 14a-b). Consistently, NPY concentration also diminished in the iWAT of HFD-induced obese mice and leptin-deficient obese mice (Supplementary Figure 14c). We can ascertain that this is not due to any changes in *Npy* expression in the ganglionic neuronal soma (Supplementary Figure 15a-b) or systemic NPY level (Supplementary Figure 4d). Altogether, these results show that obesity-induced sympathetic neuropathy reduces the NPY$^+$ innervation in the adipose tissue, and this is sufficient to decrease the local concentration of NPY in the iWAT.

We then asked if mural cells, as postsynaptic targets of NPY$^+$ innervation in iWAT, were also affected by obesity. By immunolabelling cleared iWATs for DES and CD31, we discovered that there were fewer mural cells covering the vasculature of the iWAT of DIO mice compared with age-matched lean mice (Supplementary Figure 14e-f). Since mural cells are needed for vascular integrity[39], we also observed increased vascular leakiness in the iWAT of DIO mice revealed by PV-1 staining[40] (Supplementary Figure 14g-h). To

investigate if this phenomenon is related to NPY level, we immunolabelled sympathetic ganglia for DES to ascertain if the mural cell coverage changes when the NPY level is not affected. We indeed observed that there is no significant difference in the mural cell coverage of ganglionic vasculature between DIO mice and lean mice (Supplementary Figure 15b-e), which confirms that mural cell coverage positively correlates with local NPY level.

5. Loss of function of NPY from sympathetic neurons depletes mural cells and increases vascular leakiness in adipose tissue.

To test the hypothesis that NPY^+ innervation is required for sustaining mural cells *in vivo*, we generated a mouse model in which NPY was abrogated from sympathetic neurons: Th^{Cre}; $Npy^{flox/flox}$ mice. We first confirmed that in Th^{Cre}; $Npy^{flox/flox}$ mice, NPY is knocked out from sympathetic ganglia (Supplementary Figure 16a-b) and sympathetic axons innervating iWAT and iBAT (Supplementary Figure 16c-d), while general TH^+ sympathetic innervation is not affected (Supplementary Figure 16e-f). Using this mouse model, we demonstrated that the loss of NPY in sympathetic neurons downregulated mural cell markers in the iBAT of ND-treated mice (Supplementary Figure 17a) and depleted mural cells in iBAT and iWAT of both ND-treated and HFD-treated mice (Figure 4a-c&e, Supplementary Figure 17c-d). Since mural cells are required for vascular integrity[39], we observed increased vascular leakiness in both iBAT and iWAT of Th^{Cre}; $Npy^{flox/flox}$ mice, as demonstrated by PV1-staining (Figure 4a-b). We further evaluated vascular leakiness in epidydimal WATs using an intravital method by intravenous (i.v.) injection of Dextran-70kDa. Increased vascular leakiness in Th^{Cre}; $Npy^{flox/flox}$ mice was revealed by the leak of Dextran-70kDa into the parenchyma (Supplementary Figure 17e-f), while the blood flow was unchanged (Supplementary Figure 17i). Consistent with increased vascular leakiness, we observed upregulated pro-inflammatory genes in iBAT (Supplementary figure 17b) and increased immune infiltration in iBAT and iWAT of ND-treated Th^{Cre}; $Npy^{flox/flox}$ mice (Figure 4d). These observations confirmed that NPY is required for sustaining mural cells in adipose tissue and preventing immune infiltration.

6. Loss of function of NPY from sympathetic neurons whitens iBAT before the onset of obesity, reduces beiging, energy expenditure, and thermogenesis, and renders mice intolerant to cold and more susceptible to diet-induced obesity (DIO) without increasing food intake.

To test the hypothesis that NPY locally sourced from sympathetic axons in adipose tissues preserves the mural cell pool and is required for energy homeostasis, we characterised the metabolism of Th^{Cre}; $Npy^{flox/flox}$ mice. We discovered that ND-treated lean Th^{Cre}; $Npy^{flox/flox}$ mice had whitened and bigger iBAT (Figure 5a&g), and their iBATs were dysfunctional in thermogenesis as shown by lower levels of thermogenic genes (Figure 5b).

Consistent with this, Th^{Cre}; $Npy^{flox/flox}$ mice have lower daily energy expenditure (EE) (Figure 5c, Supplementary Figure 18a) and higher respiratory exchange (RER) (Supplementary Figure 18d-e) - the latter is indicative of lower usage of fat as a metabolic substrate. By food-restricting mice, we observed that Th^{Cre}; $Npy^{flox/flox}$ mice had lower iBAT temperature, and they lost less weight during a 14-hour fast, which is indicative of energy conservation (Figure 5d-e). After 8-hour cold exposure, Th^{Cre}; $Npy^{flox/flox}$ mice have downregulated thermogenic genes in iBAT and *Prdm16* in iWAT (Supplementary Figure 18f-g) and lower rectal temperature (Supplementary figure 18h) compared with their WT littermates. It is unlikely these alterations are related to muscular activity because Th^{Cre}; $Npy^{flox/flox}$ mice have the same lean mass and locomotor activity as WT mice (Supplementary Figure 18b-c). As a cumulative result of deficient thermogenic ability and reduced EE, ND-treated Th^{Cre}; $Npy^{flox/flox}$ mice develop adult-onset obesity at the age of 30 weeks, with heavier adipose depots compared with WT mice (Figure 5f-i). When on HFD, Th^{Cre}; $Npy^{flox/flox}$ mice became obese earlier and faster than WT mice, without increasing food intake (Figure 5j-k). Also, HFD-treated Th^{Cre}; $Npy^{flox/flox}$ mice have significantly heavier adipose depots (Figure 5l-m), and their iBATs contain larger lipid droplets in average (Figure 5n, Supplementary Figure 18i). Lastly, the metabolic phenotype is invariable to gender as HFD-treated female Th^{Cre}; $Npy^{flox/flox}$ mice also have heavier body weights, WATs, and iBATs compared with $Npy^{flox/flox}$ control mice (Supplementary Figure 21b-d).

We can ascertain that the metabolic phenotypes observed in Th^{Cre}; $Npy^{flox/flox}$ mice are not caused by NPY^{+} neurons in the brain because firstly, no catecholaminergic neurons co-express NPY in hypothalamus[41] or ventral tegmental area (VTA) (Supplementary Figure 19a-d), and *Npy* expression is not changed in the hypothalamus of Th^{Cre}; $Npy^{flox/flox}$ mice (Supplementary Figure 19e); secondly, even though there is catecholaminergic neurons in the hindbrain[42], knocking out NPY from the hindbrain has no effect on thermogenesis or iBAT (Supplementary Figure 20a-g). The metabolic phenotype is also not caused by systemic NPY since NPY concentration in the blood plasma of Th^{Cre}; $Npy^{flox/flox}$ mice is unchanged (Supplementary Figure 19f). Altogether, we demonstrate that sympathetic-neuron derived NPY in adipose tissue is required for sustaining energy expenditure and leanness.

Discussion

Mural cells are contractile cells that wrap the vasculature to regulate the diameter of vessels[43] and have been described to be a source of thermogenic adipocytes both in WAT and iBAT[3-5], which are subject to the influence of NE released from adjacent sympathetic nerve terminals. These autonomic nerves co-release NPY[1,2,8], but its function in the development and activity of thermogenic adipocytes was insofar unknown. In humans, mutations in NPY

have been linked to high BMI but not an unhealthy dietary pattern[16] (https://hugeamp.org/gene.html?gene=NPY, Supplementary Figure 21a). In mice, the loss of NPY receptors leads to late-onset obesity without increases in food intake[13-15]. Taken together, the experimental evidence points to an essential role of NPY in maintaining body weight homeostasis independent of regulating appetite. Three studies have implicated NPY in directing lipogenic actions in white adipocytes, which favoured the growth of white adipose mass[24,25,27]. However, some of these studies are not replicated here[24,25], and others are not supported by modern evidence provided by our imaging data and several single-cell sequencing datasets[27]. Specifically, we show in our supplementary data that NPY neither directly promotes adipogenesis[24] nor the proliferation of 3T3-L1 pre-adipocytes[25]. Thus, the evidence disfavours a pro-obesity role for peripheral NPY, contradicting the current perception. We provide the first anatomical maps of NPY^+ innervation in white and brown adipose tissues to conclude that only one-third of sympathetic innervation is neuropeptidergic and that it preferentially targets the arterioles where mural cells exist. Consistent with recent studies showing that sympathetic axons within adipose tissues retract and degenerate with the onset of obesity[7,44], our data show that the local axonal source of NPY within these tissues is also obliterated, and this, again, refutes a direct adipogenic role of peripheral NPY. Moreover, several modern datasets omit NPY receptors in adipocytes or immune cells, whereas *Npy1r* expression is robustly detected in mural cells, identifying these cells as the postsynaptic targets of NPY^+ innervation within adipose tissues. We show that NPY sustains the mural pool of the progenitor cells of thermogenic adipocytes by promoting their proliferation and facilitates the differentiation to thermogenic adipocytes *in vitro*. *In vivo*, NPY sourced from sympathetic neurons is necessary for supporting mural cells and the normal development of thermogenic adipocytes. Conditional knockout of NPY in sympathetic neurons (NPY-cKO) depletes mural cells and whitens brown fat before the onset of obesity, rendering this tissue hypertrophic and with reduced thermogenic ability. These NPY-cKO mice have reduced thermogenic and beiging ability, lower energy expenditure, show cold intolerance and develop late-onset obesity on a regular chow diet and quickly develop obesity when fed a high-fat diet, without eating more. This metabolic phenotype matches that of NPY receptors-whole-body-knockout mice[13-15], which also develop late-onset obesity on a regular chow diet even though they eat less.

Although the effect of NPY on thermogenic adipocytes might be a combination of mural cell proliferation, differentiation and vascular leakiness, and the phenotype we observed in NPY-cKO mice might be mediated by multiple factors, being one the depletion of mural cells and inhibited neogenesis of thermogenic adipocytes, our results are the first to show the role of NPY in thermogenic adipocyte biology and clarify that central and peripheral sources of NPY have antipode roles in body weight homeostasis and the biological

mechanism described in this study is a possible explanation for why numerous mutations of the appetite-stimulating NPY paradoxically associates with high BMI in humans (https://hugeamp.org/gene.html?gene=NPY)[16] and highlights that energy dissipation may be more important than appetite in some individuals.

Figure Legends

Figure 1. A third of TH^+ sympathetic axons in iWAT and iBAT are NPY^+, and they preferentially innervate the vasculature.

(a) Confocal image of an axonal bundle dissected from the iWAT of a male lean adult mouse, stained with anti-TH (red) and anti-NPY (cyan). Scale bar=50µm.

(b) Confocal image of a capillary within a cleared iWAT of a lean adult mouse stained with anti-CD31 (red) and anti-NPY (cyan). Scale bar=100µm.

(c) Confocal images of cleared iWAT from lean adult male wildtype (WT) mice stained with anti-TH (green), anti-NPY (white), and anti-CD31 (red). Scale bar=50µm.

(d) Confocal images of cleared iWAT as in (c) from lean adult male mice stained with anti-TH (green), anti-NPY (white), and anti-CD31 (red). Scale bar=100µm.

(e-f) The quantification of images as in (d) for TH/NPY overlap: TH^+NPY^- (dark green), TH^+NPY^+ (light green), and TH^-NPY^+ (white). The percentage is shown via (e) histogram and (f) Venn diagram (n=5).

(g) The quantification of images as in (d) showing the proportion of TH^+ and NPY^+ axons overlapping with $CD31^+$ endothelial cells (n=4).

(h) Confocal Images of cleared iBAT from lean adult male mice stained with anti-TH (green), anti-NPY (white), and anti-CD31 (red).

White arrows in the images indicate TH^+NPY^- axons. Scale bar=100µm. All values are expressed as mean ± SEM, *p<0.05, **p<0.01, ***p<0.001, ****p<0.0001, Student T-tests.

Figure 2. *Npy1r* is mainly expressed in mural cells, and $NPY1R^+$ mural cells are a source of thermogenic adipocytes[3-5].

(a&c) Dot plot showing the expression of *Npy1r, Des, Myh11, Acta2 (αSMA), Tagln, Cspg4* (NG2), *Pdgfrb, Pdgfra, and Pecam1* (CD31) in the stromal vascular fraction (SVF) of (a) iWAT[22] or (c) iBAT[4].

(b&d) Embedding plots showing the expression of *Npy1r, Des, Myh11,* and *Acta2 (αSMA)* in the SVF of (b) iWAT[22] and (d) iBAT[4]. Mural cell clusters are highlighted with red rectangles or red dashed lines.

(e) The expression of *Npy1r* and *Des* in sorted $CD31^-/CD45^-/PDGFR\alpha^-/NG2^+$ mural cells and $CD45^+$ immune cells (n=5&3).

(f) Confocal image of the capillary dissected from the iWAT of WT mice stained with anti-NPY1R (cyan) and anti-CD31 (red). Scale bar=10µm.

(g) Confocal images of vessels dissected from Npy1r^{Cre}; Rosa26^{tdTomato} mice stained with anti-DES (green), Scale bar=20µm.
(h) Confocal images of vessels dissected from the iBAT of ND-treated, RT-housed 12-week-old Npy1r^{Cre}; Rosa26^{tdTomato} mice stained with anti-UCP1 (cyan), Scale bar=100 µm.
(i) Zoomed-in images of (h), scale bar=50µm.
All values are expressed as mean ± SEM, *p<0.05, **p<0.01, ***p<0.001, ****p<0.0001, Student T-tests.

Figure 3. NPY promotes proliferation of both iWAT and iBAT mural cells.
(a) Schematic of isolating mural cells from iWAT.
(b) Confocal image showing iWAT mural cells treated with or without 1µM NPY stained with DES (cyan) and DAPI. EdU (red) indicates proliferating cells. Scale bars=80µm.
(c) The percentage of EdU^{+} mural cells quantified based on images as in (B) (n=10).
(d) Schematic of isolating mural cells from iBAT.
(e) Confocal image showing iBAT mural cells treated with or without 1µM NPY stained with DES (cyan) and DAPI. EdU (red) indicates proliferating cells. Scale bars=80µm.
(f) The percentage of EdU^{+} mural cells quantified based on images as in (d) (n=3).
All values are expressed as mean ± SEM, *p<0.05, **p<0.01, ***p<0.001, ****p<0.0001, Student T-tests.

Figure 4. Loss of function of NPY from sympathetic neurons depletes mural cells and increases vascular leakiness in both iBAT and iWAT.
(a-b) Light-sheet image of cleared (a) iBAT of 15-week-old ND-treated mice (Scale bar=200µm) and (b) iWAT of 30-week-old ND-treated mice (Scale bar=500µm) stained with anti-PV1 (red) and anti-TAGLN (cyan).
(c-d) The percentage of (c) PDGFRα^{-} /NG2^{+} mural cells (n=4&2) and (d) CD45^{+} immune cells (n=2&3) in iBATs and iWATs of 30-week-old, ND-treated mice measured by flow cytometry.
(e) The percentage of DES^{+} mural cells (n=4) in iBATs and iWATs of 17-week-old, HFD-treated mice measured by flow cytometry.
All values are expressed as mean ± SEM, *p<0.05, **p<0.01, ***p<0.001, ****p<0.0001, Student T-tests.

Figure 5. Loss of function of NPY from sympathetic neurons whitens BAT before the onset of obesity, decreases energy expenditure and thermogenesis leading to adult-onset obesity on a normal diet, and renders mice more susceptible to diet-induced obesity (DIO) without increasing food intake.

(a) The picture of iBATs dissected from ND-treated 12-week-old male $Npy^{flox/flox}$ and Th^{Cre}; $Npy^{flox/flox}$ mice. The dashed lines encircle the lobes of iBATs.

(b) The expression levels of thermogenic genes *Ucp1* (n=6), *Cidea*, *Pgc1a*, and *Prdm16* (n=7), and adipogenic gene *Pparg* (n=7) in the BATs of ND-treated 12-week-old male Th^{Cre}; $Npy^{flox/flox}$ mice and $Npy^{flox/flox}$ mice.

(c) Daily energy expenditure of 7-week-old male Th^{Cre}; $Npy^{flox/flox}$ mice and $Npy^{flox/flox}$ WT mice measured using an indirect calorimetry system (n=7).

(d-e) The change in (d) iBAT temperature and (e) body weights of 12-week-old mice after a 14-hour fast (n=6 for Th^{Cre}; $Npy^{flox/flox}$ mice and n=3 for both Th^{Cre} and $Npy^{flox/flox}$ WT mice).

(f-i) The weights of (f) whole body, (h) iBATs, (h) iWATs, and (i) vWATs of ND-treated male Th^{Cre}; $Npy^{flox/flox}$ and WT mice ($Npy^{flox/flox}$) at different ages indicated in the plot (n=4).

(j-k) (j) Weekly body weights (n=8) and (k) averaged daily food consumption (n=4&6 cages) of male Th^{Cre}; $Npy^{flox/flox}$ mice and WT mice treated with HFD.

(l-m) The weights of (l) iBATs (n=5&6), (m) iWATs (n=6&7), and vWATs (n=6&7) of HFD-treated 17-week-old male Th^{Cre}; $Npy^{flox/flox}$ mice and WT mice.

(n) The average size of lipid droplets in the iBATs of ND-treated and HFD-treated male Th^{Cre}; $Npy^{flox/flox}$ mice and WT mice (n=2 for ND-treated mice, and n=4 for HFD-treated mice).

All values are expressed as mean ± SEM, *p<0.05, **p<0.01, ***p<0.001, ****p<0.0001, Student T-tests.

Method

1. Animals

Th^{Cre} mice (B6.Cg-*7630403G23Rik*$^{Tg(Th\text{-}cre)1Tmd}$/J; stock no. 008601), $Cx3cr1^{GFP/+}$ mice (*Cx3cr1*^{tm1Litt}/LittJ; stock no. 008451) were purchased from the Jackson Lab (JAX). $Npy^{flox/flox}$ mice were a donation from Ivo Kalajzic Lab at the Department of Reconstructive Science, University of Connecticut[45] under MTA. Tissues of NPY-GFP mice (B6.FVB-Tg(Npy-hrGFP)1Lowl/J) are from Tamas Horvath Lab at Brandy Memorial Laboratory, Yale University. Tissue of $Npy1r^{Cre}$; $Rosa26^{tdTomato}$ mice were from Professor Michael Roberts at Department of Otolaryngology-Head and Neck Surgery, University of Michigan. Sympathetic neuron-specific NPY-cKO mice were generated by crossing Th^{Cre} mice with $Npy^{flox/flox}$ mice. Diet-induced obesity (DIO) was achieved by feeding mice an HFD (Diet Research, D12492) when they were 7 weeks old, and lasted for 10 weeks. The body weight of each mouse and the food consumption in each cage were recorded weekly. All the mice were group housed in standard housing under a 12-12-hour light-dark cycle and given access to diet and water *ad libitum*. All experimental procedures were performed on living animals in accordance with the United Kingdom ANIMALS ACTS 1986 under the project license (PPL number: P80EDA9F7) and

personal licenses granted by the United Kingdom Home Office. Ethical Approval was provided by the Ethical Review Panel at the University of Oxford.

2. Energy expenditure and respiratory exchange rate measurement

Animals with 6 weeks were analyzed for Oxygen Consumption (V_{O2}), Carbon Dioxide Production (V_{CO2}), Energy Expenditure (EE) and Respiratory Exchange Rate (RER) using an indirect calorimetry system (Panlab; Harvard Apparatus; LE405 Gas Analyzer and Air Supply & Switching). Animals were maintained in individual cages, following a 12h light/dark cycle, with water and food supplied *ad libitum*, and controlled room temperature (21-23ºC) and humidity. Metabolic data was collected for five days, after two-days acclimatation period. Animal's body weight (g) and food (g) were measured before entering, and after exiting the cage. Results were normalized by weight, and graphs and statistical analysis were obtained using the CalR Web-based Analysis Tool for Indirect Calorimetry Experiments[46].

3. Locomotor activity and body composition measurement

Animals with 8-9 weeks were analyzed for spontaneous locomotor activity (Panlab; Harvard Apparatus; LE001 PH Multitake Cage). Animals were maintained in individual cages, following a 12h light/dark cycle, with water and food supplied *ad libitum*, and controlled room temperature (21-23ºC) and humidity. Data was collected for 72 hours, after one-day acclimatation period. Activity was recorded by COMPULSE v1.0 Software (PanLab). Animals with 7-9 weeks were analyzed for body composition using Minispec LF50 (Brucker).

4. Fasting and thermoimaging

Animals with 12-14 weeks were used for thermoimaging. Data in Figure 5E were recorded using Optris thermo-cameras (Optris PI 160 with standard 61 lens, Optris GmbH, Berlin, Germany), and Data in Supplementary Figure 16F were recorded using an FOTRIC 225s infrared camera and analysed using FOTRIC software. Animals were single-housed and put under the thermo-cameras, and their backs were shaved to expose skin above iBATs. Animals were acclimatised for 4 days in individual cages with *ad libitum* access to food and water at room temperature under a 12/12 light-dark cycle before a 14-hour fast. Mice have *ad libitum* access to water during fasting.

iBAT temperature was recorded every second for a 6-day period by storing the temperature of the warmest pixel in view using the software provided by the camera's manufacturer (Optris PIX Connect, Optris GmbH). The iBAT temperature at 0 and 14 hours was an average of temperatures during a1-hour period.

5. Cold-exposure experiment.

Animals with 20 weeks were single-housed in a thermoneutral environment (31 □, 50% humidity) under 12/12 light-dark cycle for a week, with *ad libitum* access to food and water. Afterwards, the mice were cold-challenged at 4□, and their rectal temperature were measured every hour using a rectal probe. Animals were sacrificed immediately after 8-hour cold-exposure, and their iBATs were harvested for RT-qPCR analysis.

6. Stereotaxic injection

For viral injection, mice were anaesthetized with avertin (240mg/kg, i.p.) and fixed on a stereotaxic holder (RWD, Life Science, China). AAV2/9-hSyn-Cre-EGFP-WPRE-pA (Taitool, S0230-9, 2×1012 V.G./mL, 200nl for each side) or AAV2/9-hSyn-EGFP-WPRE-pA (Cat#S0237-9, Taitool, 2×1012 V.G./mL, 200nl for each side) was bilaterally injected into the NTS (NTS coordinate AP/ML/DV: -7.5/±0.35/-4.75 mm) of $Npy^{flox/flox}$ mice.

7. Immunofluorescent staining (IF)

Superior cervical ganglia (SCG) and sympathetic axon bundles were dissected adipose tissues of mice perfused with 20mL PBS and fixed in 4% paraformaldehyde (ThermoFisher, 043368.9M) for at least 4 hours. Cells collected after *in vitro* experiments were washed once with PBS and fixed using 4% PFA for at least 4 hours. Axon bundles were stained by first incubating with primary antibodies dissolved in the permeabilising buffer (3% BSA, 2% goat serum, 0.1% triton x-100, and 0.1% sodium azide in PBS) overnight at 4 □, followed by incubation with secondary antibodies and DAPI dissolved in the permeabilising buffer for 1 hour with gentle agitation. As for IF in fixed cells, cells were first incubated with the permeabilising buffer for 1 hour at room temperature (RT), and then stained at 4□ overnight with primary antibodies diluted in the permeabilising buffer. Then, samples were washed and stained with DAPI and secondary antibodies for 1 hour at RT. Sympathetic fibres or fixed cells were then mounted on slides with Fluoromount-G mounting medium (ThermoFisher, 00-4958-02).

For cryosection, samples were first embedded in OCT (VWR, 361603E) and frozen at -20□ until cryosectioning. Samples were cut into 10 µm-thick sections and mounted on charged SuperFrost Plus slides (VWR, 631-0108). Afterwards, the samples were stained using the same procedure as fixed cells.

For paraffin-embedding, fixed samples were processed in 70%, 80%, and 90% ethanol, and then in 100% ethanol, 100% xylene, and 60□ paraffin wax 3 times for each condition. The samples were embedded in paraffin wax, sectioned at 7µm, mounted on coverslips, and dried with 45-50□ oven overnight. Before staining, samples were deparaffinised in 100% xylene for 5 minutes twice and rehydrated twice in 100% ethanol, then once in 95%, 80% ethanol, and water for 10 minutes each. Antigen retrieval was done by adding 0.05% Trypsin to each slide and incubating at 37□ for 20 minutes. After

washing with running water, the samples were stained using the same procedure as fixed cells.

For whole-mount ganglia staining, PFA-fixed ganglia were dehydrated in 30%, 50%, 70%, and 90% once and twice in 100% ethanol, and the ganglia were 70kept shaking for 20 minutes at each concentration, and then ganglia were rehydrated in 90%, 70%, 50%, and 30% ethanol. Afterwards, ganglia were digested with 1.5 U/mL dispase-1 (Roche- 04942078001), 0.5 mg/mL collagenase (Sigma, C2674), and 300 µg/mL hyaluronidase (Sigma, H3884) diluted in PBS, shaking in 37 □ water bath for 30 minutes. Ethanol-treated ganglia were blocked in blocking solution (3% BSA, 2% goat serum, 0.1% triton x-100, and 0.1% sodium azide in PBS) for 2 hours and then incubated with primary antibodies diluted in the permeabilising buffer for 3 days at 4□. 3 days later, ganglia were incubated in secondary antibodies diluted in the permeabilising buffer for another 3 days at 4□. Finally, ganglia were dehydrated in 30%, 50%, 70%, 90% ethanol and twice in 100% ethanol, and were cleared using ethyl cinnamate (ECi). Cleared ganglia were mounted in a coverslip-slide sandwich filled with ECi.

Images were acquired using a Zeiss LSM880 confocal microscope with Zen-black software (V2.1). The samples were imaged using a 10x/0.45NA objective, with a 1.04 µm, 1.04 µm, 3.64 µm xyz voxel size, a 20x/0.8NA objective, with a 0.52 µm, 0.52 µm, 1.00 µm xyz voxel size, or a 63x/1.4NA oil-immersion objective, with a 0.13 µm, 0.13 µm, 1.00 µm xyz voxel size. Solid-state 405nm, 561nm, 633nm, and Argon 488 lasers were used for DAPI, AF488, AF546, and AF647 fluorophores respectively.

8. Adipose Tissue Clearing

Whole fat pads were stained and cleared using a modified version of iDISCO as previously described[18,47]. Briefly, white adipose tissues (WATs) were dissected from mice perfused with 20mL PBS and fixed with 4% paraformaldehyde overnight. Tissues were pre-treated with 20%, 40%, 60%, 80% and twice in 100% methanol for 30 minutes each at RT, and then bleached using 5% H_2O_2 diluted in 100% methanol for 24 hours at 4 □ shaking. Bleached samples were rehydrated using 80%, 60%, 40%, and 20% methanol for 30 minutes each and then in PTwH buffer (0.2% Tween-20, 10µg/mL heparin, and 0.02% sodium azide in PBS) for 30 minutes. Afterwards, samples were incubated in permeabilising solution (20% DMSO, 0.2% Triton x-100, 0.3M glycine in PBS) at 37□ water bath overnight and blocked using blocking buffer (10% DMSO, 2% Triton x-100, 0.02% sodium azide and 5% goat serum in PBS). For immunolabeling, samples were incubated in primary antibodies diluted in antibody dilution buffer (5% DMSO, 5% goat serum, 0.2% Tween-20 and 10 µg/mL heparin in PBS) at 37□ shaking for 5 days, then washed with PTwH for 1 day, and then incubated with secondary antibodies and DAPI diluted using antibody dilution buffer at 37□ shaking for another 3 days. Immunolabelled tissues were embedded in 1%

agarose and dehydrated in 20%, 40%, 60%, 80%, and 100% methanol for 1 hour each, and then 100% overnight at room temperature. Samples were incubated in dichloromethane (DCM) (Sigma, 270997) until they sank, and then incubated in dibenzyl ether (DBE) (Sigma, 179272) until clear. Samples were stored in DBE at room temperature, and transferred into ECi before imaging. Images of cleared tissues were required using a Myltenyi Biotec Ultramicroscope II light-sheet microscope. The step size was 8µm; the thickness of the light sheet was 3.98 µm; the horizontal dynamic focusing was set to 8 steps; and the exposure time was set at 180ms. The samples were illuminated using a bi-directional light-sheet and scanned under a 2x/0.5 NA objective, with a 4.03 µm, 4.03 µm, 8 µm xyz voxel size. A 488nm laser with a 525/50 filter, a 561nm laser with a 620/60 filter, and a 638nm laser with a 680/30 filter were used for AF488, AF546, and AF647 respectively.

9. Dextran-70kDa injection and intravital microscopy.

Animals were anesthetized with ketamine (100mg/kg) and xylazine (10mg/kg) and a small incision was made to expose de epididymal adipose tissue (eWAT) for microscope analysis. Intravital images with space resolution (1024x1024 pixels) from eWAT were obtained by Optical microscope CARS (Coherent Anti-stokes Raman Scattering), TPEF (Two-photon excitation fluorescence) and Bright-field microscope, simultaneously, using confocal LSM 780-NLO Zeiss in the inverted microscope Axio Observer Z.1 (Carl Zeiss AG, Alemanha). All the procedures were performed in the National Institute of Science and Technology on Photonics Applied to Cell Biology (INFABIC) at the State University of Campinas. The adipocyte images from CARS were acquired using two lines of lasers in a wavelength of λpump=803 nm e λStokes=1040 nm, and fluorescence images were acquired by TPEF using exogenous fluorescence dye Tetramethylrhodamine isothiocyanate dextran (Sigma, cat. # T1162) in wavelength of excitation of λStokes=1040 nm. After the identification of a blood vessel and acquisition of an initial image, the video was started and after 10 frames, 50ul (30mg/kg) of Dextran 70KDa (Sigma, cat. # T1162) was injected in the orbital plexus of the mice. The video continued recording for approximately 12 minutes to capture vessel fluorescence and leakage. Fluorescence intensity over time was analysed for the whole duration of the video. A static image was analysed after dextran administration using FIJI[48]. To evaluate tissue leakage, a ROI was selected inside the vessel and another ROI was selected in the tissue (outside the vessel). Fluorescence intensity was measured in both areas. The intensity ratio between the tissue and inside the vessel was calculated. Blood flow was calculated using the average of the raw intensity of Dextran inside the artery over 100 seconds right after the stabilization of the Dextran signal following administration.

10. Antibodies

The following primary antibodies were used for immunofluorescent staining: rat anti-CD31 (BioLegend, 102501 ,MEC13.3,1:100 dilution), rat anti-PLVAP (BioLegend, 120503, MECA32, 1:100 dilution), rabbit anti-DES (Abcam, AB15200, 1:500 dilution), rabbit anti-NPY (Cell Signalling, D7Y5A, 1:500 dilution), rabbit anti-NPY (Abcam, AB30914, 1:500 dilution), chicken anti-TH (Aves Labs, TYH73787982, 1:500 dilution), rabbit anti-TH (Sigma, Ab152, 1:500 dilution), mouse anti-NPY1R (Santa Cruz, sc-393192, 1:200 dilution), rat anti-PDGFRα (BioLegend, 135902, APA5, 1:200 dilution), rabbit anti-TAGLN (Abcam, AB14106, 1:250 dilution), Cy3 anti-αSMA (Sigma, C6198, 1A4, 1:250 dilution), goat anti-SOX17 (R&D, AF1924, 1:250), goat anti-EPHB4 (R&D, AF3034, 1:250), rabbit anti-UCP1 (Abcam, Ab10983, 1:500).
The following antibodies were used for FACS and flow cytometry: AF700 anti-CD45 (BioLegend, 103128), BUV395 anti-CD45 (BioLegend, 564279), Pacific Blue anti-CD31 (102421), APC anti-PDGFRa (BioLegend 135907), AF488 anti-NG2 (Sigma, MAB5384A4), and AF488 anti-DES (Abcam, AB185033, Y66). LIVE/DEAD™ Fixable Near-IR Dead Cell Stain Kit (ThermoFisher, L10119) was used for live/dead staining.

11. qPCR

RNA extraction was performed using Trizol reagent (Thermofisher, 15596026), cDNA was synthesized using SuperScript II Reverse Transcriptase (Invitrogen, 18064022), and qPCR was done using Power SYBR Green PCR Master Mix (LifeTech 4368706).
The following primers were used in this research:

Table 1. The Sequence of Primers for RT-qPCR

Gapdh	Forward	5'-AACTTTGGCATTGTGGAAGG-3'
	Reverse	5'-ACACATTGGGGGTAGGAACA-3'
Hprt	Forward	5'-CAGTCCCAGCGTCGTGATTA-3'
	Reverse	5'-TGGCCTCCCATCTCCTTCAT-3'
Plin1	Forward	5'-TAGAGTTCCTCCTGCCACCA-3'
	Reverse	5'-GTGCTGACCCTCCTCACAAG-3'
Pparg	Forward	5'-TCAAGGGTGCCAGTTTCG-3'
	Reverse	5'-GGAGGCCAGCATCGTGT-3'
Des	Forward	5'-TCCAGTCCTACACCTGCGAGAT-3'
	Reverse	5'-CGCAATGTTGTCCTGATAGCCA-3'
Npy	Forward	5'-CCCCAGAACAAGGCTTGAAG-3'

	Reverse	5'-TTGGAAAAGTCGGGAGAACAA-3'
Npy1r	Forward	5'-CTGATGGACCACTGGGTCTT-3'
	Reverse	5'-GAAGAAGCCACTGCAAGGAC-3'
Npy2r	Forward	5'-ATCATCTTGCTAGGGGTAGTTGG-3'
	Reverse	5'-CGGACCCATTTTCCACTCTCC-3'
Npy5r	Forward	5'-GTGAACTTTCTCATAGGCAACCT-3'
	Reverse	5'-GCATGATATGGCACATGGCTTT-3'
Pdgfrb	Forward	5'-AGGACAACCGTACCTTGGGTGACT-3'
	Reverse	5'-CAGTTCTGACACGTACCGGGTCTC-3'
Rgs5	Forward	5'-CAAAATGGCGGAGAAGGCAA-3'
	Reverse	5'-CCAAGTCAAAGCTGCGAGGA-3'
Tgfb1	Forward	5'-TGATACGCCTGAGTGGCTGTCT-3'
	Reverse	5'-CACAAGAGCAGTGAGCGCTGAA-3'
Cidea	Forward	5'-TGCTCTTCTGTATCGCCCAGT-3'
	Reverse	5'-GCCGTGTTAAGGAATCTGCTG-3'
Pgc1a	Forward	5'-CCCTGCCATTGTTAAGAC-3'
	Reverse	5'-TGCTGCTGTTCCTGTTTTC-3'
Ucp1	Forward	5'-ACTGCCACACCTCCAGTCATT-3'
	Reverse	5'-CTTTGCCTCACTCAGGATTGG-3'
Prdm16	Forward	5'- CAGCACGGTGAAGCCATT-3'
	Reverse	5'-GCGTGCATCCGCTTGTG-3'
Serca2b	Forward	5'-ACCTTTGCCGCTCATTTTCCAG-3'
	Reverse	5'-AGGCTGCACACACTCTTTACC-3'
Angpt1	Forward	5'-TGCAGCAACCAGCGCCGAAA-3'
	Reverse	5'-CACGGCAGTTCCCGTCGTGT-3'
Tnf	Forward	5'- ATGAGCACAGAAAGCATGA-3'
	Reverse	5'- TACAGGCTTGTCACTCGAA-3'

Il6	Forward	5'-ACGGCCTTCCCTACTTCACA-3'
	Reverse	5'- CATTTCCACGATTTCCCAGA-3'

ΔCt method was used to quantify gene expression using the formula: relative expression = 2^(-($Ct_{target\ gene}$-$Ct_{reference\ gene}$)). ΔΔCt method was used to compare thermogenic and adipogenic gene expression shown in Figure 5b, Supplementary Figure 11, 18f&g, and 20g.

qPCR data shown in Supplementary Figure 20g was collected using CFX96 Real-Time PCR Detection System (Bio-Rad) with TB Green Premix Ex Taq II (Cat# RR820A, TaKaRa).

12. Protein extraction and blood plasma isolation for NPY ELISA

Proteins were extracted from iWATs as previously described in a published paper[49]. Briefly, dissect iWATs were put in homogenising tubes filled with 300μL/50mg RIPA lysis buffer (Sigma, 20188) containing 50μM DPP-IV inhibitor (Sigma, DPP4-010) and 500KIU/mL Aprotinin (Sigma, A6103-1MG) and homogenised using Precellys 24 homogeniser. The lipid in the tissue homogenise was removed by centrifuging the tissue homogenise at 20000x rcf at 4□ for 15 minutes, and the clear part was kept. The process was repeated 3 times to completely remove lipids.

To do terminal blood collection, the mice were euthanised by i.p. injection with 10 μL/g pentobarbital, and then blood was collected from the left ventricle using 25G needles and syringes coated with 100 mM EDTA. The blood was then put into tubes with 5 μL 100mM EDTA and centrifuged at 1000x rgf at 4□ for 15 minutes to separate blood plasma from blood cells, and then the supernatant was moved to new tubes with DPP-IV inhibitor (final concentration 50 μM) and Aprotinin (final concentration 500 KIU/mL). The concentration of NPY in the iWAT and blood plasma of mice was determined using an NPY ELISA kit (Merck, EZRMNPY-27K).

13. Single-cell suspension and flow cytometry

Dissected adipose tissues were minced and digested in the enzyme mixture (for each sample, 500μL Collagenase II (4mg/mL, C6885), 500μL Hyaluronidase (5.3mg/mL=40000U/mL, H3884), and 5μL Dnase I (BioLabs, M0303L)) in a 37 □-water bath shaking for 45 minutes, and samples were pipetted every 10 minutes. Digestion was stopped by adding FACS buffer (PBS containing 2% FBS), and single-cell suspension was collected by filtering the digested sample using EASYStrainer cell sieves with 70μm mesh (Greiner, 542070).

To prepare the samples for sorting or flow cytometry, cells were first treated with red-blood-cell lysis buffer (BioLegend, 420301) to remove red-blood cells, and treated with Fc block (ThermoFisher, 14-9161-73) before staining with

antibodies. Before immunolabelling for intracellular markers, cells were fixed and permeabilised using the eBioscience Intracellular Fixation and Permeabilization Buffer Set (ThermoFisher, 88-8824-00). Cell sorting was done using a BD FACSAria III sorter, and flow cytometry data were acquired using a BD FACSAria III sorter or a BD LSRFortessa X20 cytometer with a BD FACSDiva v6.0 software. Cytometry data were analysed using FlowJo v10.8.1.

14. Isolation and primary culture of mural cells and *in vitro* stimulation.

Mural cells were isolated and cultured following a modified version of the protocol previously published[50]. Briefly, the mice were euthanised by i.p. injection with 10μL/g pentobarbital and perfused with 15mL PBS to remove blood. The stromal vascular fraction (SVF) of the iBATs was isolated using the method described above. Then, the cells were seeded in 10cm dishes with 10mL DMEM with 10% FBS for 2 days for the cells to attach to the bottom. Afterwards, 5mL of the medium was replaced with mural cell-specific medium (DMEM with 2% FBS supplied with 1% mural cell-growth supplement (Science Cell, 1252)). 5mL of the medium in the dishes was refreshed every 2 days until the cell grow confluent. To get pure mural cells, cells were labelled with an APC anti-CD104b antibody (BioLegend, 136007), and mural cells were sorted using MojoSort™ magnetic sorting protocol with MojoSort™ buffer (BioLegend, 480017) and anti-APC nanobeads (BioLegend, 480071).

To perform *in vitro* co-culturing experiments. The cells were seeded at 5x10^4cells/mL on glass coverslips and indicated concentration of PDGF-BB (R&B, 220-BB) and NPY (Cayman Chemical, CAY15071) were added to the cells 24 hours after the cells were seeded. Finally, the cells were collected 5 days later and either fixed with 4% PFA for imaging or lysed with Trizol for RNA extraction and qPCR.

15. Cell lines

RAW264.7 murine macrophage cell line (Sigma, 91062702) was purchased from Sigma. The complete medium for culturing the cells includes high glucose DMEM with glutamate (Sigma, 41965039) and 10% FBS (Sigma, 12133C).

The 3T3-L1 preadipocyte cell line was a gift from Associate Professor Robin Klemm at the Department of Physiology, Anatomy and Genetics, University of Oxford. The complete medium for culturing the cells includes high glucose DMEM with glutamate (ThermoFisher, 41965039) and 10% calf serum (Sigma, 12133C). To subculture preadipocytes, the medium was moved, and cells were washed with 1mL pre-warmed 0.05% trypsin (ThermoFisher, 25300054), and digested with 200μL trypsin at 37□ for 5-10 minutes. Afterwards, digestion was stopped, and cells were resuspended using the complete medium.

16. Induction to white and thermogenic adipocytes

To differentiate 3T3-L1 cells to white adipocytes, cells were seeded in 12-well plates at a density of 1x10^5cells/mL. Medium was refreshed until the cells were confluent. 2 days after the cells were confluent, induction medium (10% FBS, 500μM 3-Isobutyl-methylxanthine and 1μM dexamethasone in DMEM) with or without 1μg/mL insulin were added into each well. 3 days later, the induction medium was replaced with the maintenance medium (DMEM with 10% FBS and with or without 1 μg/mL insulin). Afterwards, medium was refreshed with the maintenance medium every 2 days. The total differentiation time for each well was 8 days. NPY treatments in the experimental groups starts when the induction medium was added and lasted through the whole differentiation process.

SVF and mural cells was differentiated to thermogenic adipocytes as previously published[5,30]. SVF and mural cells was isolated and seeded in 12-well plates at a density of 1x10^5cells/mL. When cells reach 95% confluency, beige cell induction medium (DMEM with 10% FBS, 125μM Indomethacin, 5 μM Dexamethasone, 500μM 3-Isobutyl-methylxanthine, and 0.5μM Rosiglitazone) was added to each well. 2 days later, the induction medium was replaced with maintenance medium (DMEM with 10% FBS, 5μg/mL Insulin, and 1nM Triiodothyronine). Afterwards, the maintenance medium was refreshed every 2 days. The total differentiation time for each well was 8 days. NPY treatments in the experimental groups started when the induction medium was added and lasted through the whole differentiation process. Oxygen consumption was measured using a Seahorse XF Analyzer.

17. Cell proliferation assay.

Cell proliferation assay was done with Click-iT EdU Cell Proliferation Kit for imaging (C10340). Mural cells were seeded at 0.5x10^5 cells/ml in 12-well plates on coverslips and cultured overnight before the experiments. Afterwards, cells were labelled with EdU and cultured with or without 1 μM NPY or 2μM PD98059 (Cell Signalling 9900S) for 6 hours in medium for mural cells (low-glucose DMEM with 2%FBS). Cells were then fixed with 4% PFA and permeabilising buffer for 30 minutes respectively, and EdU was labelled with AF647 using Click-iT® Plus reaction cocktail. After IF staining with anti-DES, cells were imaged using a Zeiss LSM880 confocal microscope with Zen-black software (V2.1), with a 20x/0.8NA objective, a 0.52 μm, 0.52 μm, 1.00 μm xyz voxel size. An area of 3072x3072 pixels were imaged for each biological replicate.

18. scRNA-Seq dataset analysis

Public scRNA-Seq datasets were downloaded from GEO, and were analysed using the following method. Cells with <200 unique detected genes or >5% mitochondrial counts were discarded. After filtering, the gene x cell matrix was

normalised using 'NormalizeData()' in Seurat v4.2.0[51] in R (v4.2.2) environment. Then, the data were scaled using 'ScaleData()', and we performed linear dimensional reduction by PCA and calculated UCMP coordinates for all cells using Seurat v4.2.0. The cells were clustered using 'FindNeighbour()', with dimensions set to 15 and 'FindClusters()', with resolution set to 0.5. Each cluster were identified based on differentially expressed genes and known markers in published literatures[4,22,29,52-54].

19. Figure quantification

The overlapping between TH, NPY and CD31 was calculated using JACoP[55], a plugin in FIJI[48]. To make this calculation, 472.33μm, 472.33μm, 30μm xyz regions were randomly picked and maximally project to z using Fiji script. The labelled areas were automatically segmented using threshold set by default, and the overlapping percentages were calculated automatically by JACoP. 5 views from 3 biological replicates for iWAT were quantified.

The innervation of NPY^+ axons was quantified using the "Surface" tool in ImarisV9.2. The labelled area of NPY^+ axons and $CD31^+$ vessels in whole cleared iWATs were automatically segmented, and the innervation of NPY in vasculature was calculated as $Volume_{NPY}^+/Volume_{CD31}^+$. The coverage of DES^+ mural cells in iWAT was calculated similarly as $Volume_{DES}^+/Volume_{CD31}^+$. Confocal images showing NPY^+ innervation were quantified using FIJI with an automatic unbiased method. $Area_{NPY+}$ and $Area_{CD31+}$ were segmented using Otsu thresholding method and measured using "measure" program.

The percentage of EdU^+ cells were counted with an unbiased automatic method using "detect particles" in FIJI[48]. Threshold was set automatically using Otsu thresholding method. 10 views from 10 biological replicates were used for quantification.

The percentage of $PDGFR\alpha^+$ and DES^+ cells were count manually based on the PDGFRα and DES signals. The percentage of TH^+ and NPY^+ neurons in hypothalamus and VTA was also counted manually. To calculate the ganglionic mural cell coverage, 531μm, 531μm, 30μm xyz views were randomly picked and maximally project to z using Fiji script. The labelled areas were segmented using threshold set by default, and the coverage was calculated as $Area_{NPY}^+/Area_{CD31}^+$. 11 views from 4 biological replicates were quantified for each condition.

The size of adipocytes in WAT and iBAT was quantified as previously described[56] using FIJI. Briefly, WAT and iBAT were processed to paraffin-embedded sections (3μm sections), stained with H&E and scanned into digital images using a NanoZoomer-SQ Digital slide scanner -Hamamatsu. Images were randomly picked and the plugin Analyse Particles was used to count the number and measure the size of adipocytes and droplets in iBAT. For each iBAT, 11000 lipid droplets were measured.

20. Statistics

GraphPad Prism v.9.5.0 was used for statistical analysis. Mean and standard error of the mean (SEM) were used to represent a sample. Chi-Square Test and paired two-tailed Student T-test were used to compare two samples; ANOVA was used to compare multiple data points.

Data Availability

The scRNA-Seq datasets of iWAT and iBAT were deposited on the Gene-Expression Omnibus under the accession numbers GSE154047 and GSE160585. All the numeric data for supporting this research are available within the paper and the Supplementary information.

Code Availability

The code used for scRNA-Seq analysis is deposited at Github (https://github.com/PLAVRVSO/scRNA-Seq-analysis-of-iBAT-SVF).

Reference

1 LUNDBERG, J. M. *et al.* Neuropeptide Y (NPY)-like immunoreactivity in peripheral noradrenergic neurons and effects of NPY on sympathetic function. *Acta Physiologica Scandinavica* **116**, 477-480 (1982).

2 Lundberg, J., Franco-Cereceda, A., Hemsen, A., Lacroix, J. & Pernow, J. Pharmacology of noradrenaline and neuropeptide tyrosine (NPY) - mediated sympathetic cotransmission. *Fundamental & clinical pharmacology* **4**, 373-391 (1990).

3 Long, J. Z. *et al.* A smooth muscle-like origin for beige adipocytes. *Cell metabolism* **19**, 810-820 (2014).

4 Shamsi, F. *et al.* Vascular smooth muscle-derived Trpv1+ progenitors are a source of cold-induced thermogenic adipocytes. *Nature metabolism* **3**, 485-495 (2021).

5 Oguri, Y. *et al.* CD81 controls beige fat progenitor cell growth and energy balance via FAK signaling. *Cell* **182**, 563-577. e520 (2020).

6 Caron, A., Lee, S., Elmquist, J. K. & Gautron, L. Leptin and brain–adipose crosstalks. *Nature Reviews Neuroscience* **19**, 153-165 (2018).

7 Zeng, W. *et al.* Sympathetic neuro-adipose connections mediate leptin-driven lipolysis. *Cell* **163**, 84-94 (2015).

8 Ekblad, E. *et al.* Neuropeptide Y co-exists and co-operates with noradrenaline in perivascular nerve fibers. *Regulatory peptides* **8**, 225-235 (1984).

9 Le Roux, C. & Bloom, S. Peptide YY, appetite and food intake. *Proceedings of the Nutrition Society* **64**, 213-216 (2005).

10 Stanley, B. G. & Leibowitz, S. F. Neuroreptide Y: Stimulation of feeding and drinking by injection into the paraventricular nucleus. *Life sciences* **35**, 2635-2642 (1984).

11 Marie, L. S., Luquet, S., Cole, T. B. & Palmiter, R. D. Modulation of neuropeptide Y expression in adult mice does not affect feeding. *Proceedings of the National Academy of Sciences* **102**, 18632-18637 (2005).

12 Erickson, J. C., Clegg, K. E. & Palmiter, R. D. Sensitivity to leptin and susceptibility to seizures of mice lacking neuropeptide Y. *Nature* **381**, 415-418 (1996).

13 Naveilhan, P. *et al.* Normal feeding behavior, body weight and leptin response require the neuropeptide Y Y2 receptor. *Nature medicine* **5**, 1188-1193 (1999).

887 14 Pedrazzini, T. *et al.* Cardiovascular response, feeding behavior and locomotor activity
888 in mice lacking the NPY Y1 receptor. *Nature medicine* **4**, 722-726 (1998).
889 15 Nguyen, A. D. *et al.* Y1 and Y5 receptors are both required for the regulation of food
890 intake and energy homeostasis in mice. *PloS one* **7**, e40191 (2012).
891 16 Dornbos, P. *et al.* Evaluating human genetic support for hypothesized metabolic
892 disease genes. *Cell metabolism* **34**, 661-666 (2022).
893 17 Furlan, A. *et al.* Visceral motor neuron diversity delineates a cellular basis for nipple-
894 and pilo-erection muscle control. *Nature neuroscience* **19**, 1331-1340 (2016).
895 18 Chi, J., Crane, A., Wu, Z. & Cohen, P. Adipo-clear: a tissue clearing method for three-
896 dimensional imaging of adipose tissue. *JoVE (Journal of Visualized Experiments)*,
897 e58271 (2018).
898 19 Wang, H. U., Chen, Z.-F. & Anderson, D. J. Molecular distinction and angiogenic
899 interaction between embryonic arteries and veins revealed by ephrin-B2 and its
900 receptor Eph-B4. *Cell* **93**, 741-753 (1998).
901 20 Kim, D. *et al.* Sox17 mediates adult arterial endothelial cell adaptation to
902 hemodynamics. *Biomaterials* **293**, 121946 (2023).
903 21 Singer, K. *et al.* Neuropeptide Y is produced by adipose tissue macrophages and
904 regulates obesity-induced inflammation. *PloS one* **8**, e57929 (2013).
905 22 Henriques, F. *et al.* Single-cell RNA profiling reveals adipocyte to macrophage
906 signaling sufficient to enhance thermogenesis. *Cell reports* **32**, 107998 (2020).
907 23 Attwell, D., Mishra, A., Hall, C. N., O'Farrell, F. M. & Dalkara, T. What is a pericyte?
908 *Journal of Cerebral Blood Flow & Metabolism* **36**, 451-455 (2016).
909 24 Rosmaninho-Salgado, J. *et al.* Intracellular mechanisms coupled to NPY Y2 and Y5
910 receptor activation and lipid accumulation in murine adipocytes. *Neuropeptides* **46**,
911 359-366 (2012).
912 25 Yang, K., Guan, H., Arany, E., Hill, D. J. & Cao, X. Neuropeptide Y is produced in
913 visceral adipose tissue and promotes proliferation of adipocyte precursor cells via
914 the Y1 receptor. *The FASEB Journal* **22**, 2452-2464 (2008).
915 26 Chen, W.-c. *et al.* Neuropeptide Y is an immunomodulatory factor: direct and
916 indirect. *Frontiers in immunology* **11**, 580378 (2020).
917 27 Kuo, L. E. *et al.* Neuropeptide Y acts directly in the periphery on fat tissue and
918 mediates stress-induced obesity and metabolic syndrome. *Nat Med* **13**, 803-811,
919 doi:10.1038/nm1611 (2007).
920 28 Yan, C. *et al.* Peripheral-specific Y1 receptor antagonism increases thermogenesis
921 and protects against diet-induced obesity. *Nat Commun* **12**, 2622,
922 doi:10.1038/s41467-021-22925-3 (2021).
923 29 Emont, M. P. *et al.* A single-cell atlas of human and mouse white adipose tissue.
924 *Nature* **603**, 926-933 (2022).
925 30 Aune, U. L., Ruiz, L. & Kajimura, S. Isolation and differentiation of stromal vascular
926 cells to beige/brite cells. *JoVE (Journal of Visualized Experiments)*, e50191 (2013).
927 31 Hansel, D., Eipper, B. & Ronnett, G. Neuropeptide Y functions as a neuroproliferative
928 factor. *Nature* **410**, 940-944 (2001).
929 32 Medeiros, P. J., Pascetta, S. A., Kirsh, S. M., Al-Khazraji, B. K. & Uniacke, J. Expression
930 of hypoxia inducible factor–dependent neuropeptide Y receptors Y1 and Y5
931 sensitizes hypoxic cells to NPY stimulation. *Journal of Biological Chemistry* **298**
932 (2022).
933 33 Shimada, K. *et al.* Neuropeptide Y activates phosphorylation of ERK and STAT3 in
934 stromal vascular cells from brown adipose tissue, but fails to affect thermogenic
935 function of brown adipocytes. *Peptides* **34**, 336-342 (2012).
936 34 Zhang, W. & Liu, H. T. MAPK signal pathways in the regulation of cell proliferation in
937 mammalian cells. *Cell research* **12**, 9-18 (2002).

938 35 Armulik, A., Genove, G. & Betsholtz, C. Pericytes: developmental, physiological, and
939 pathological perspectives, problems, and promises. *Dev Cell* **21**, 193-215,
940 doi:10.1016/j.devcel.2011.07.001 (2011).
941 36 Hosaka, K. *et al.* Pericyte-fibroblast transition promotes tumor growth and
942 metastasis. *Proc Natl Acad Sci U S A* **113**, E5618-5627, doi:10.1073/pnas.1608384113
943 (2016).
944 37 Onogi, Y. *et al.* PDGFRbeta Regulates Adipose Tissue Expansion and Glucose
945 Metabolism via Vascular Remodeling in Diet-Induced Obesity. *Diabetes* **66**, 1008-
946 1021, doi:10.2337/db16-0881 (2017).
947 38 Wang, P. *et al.* A leptin-BDNF pathway regulating sympathetic innervation of adipose
948 tissue. *Nature* **583**, 839-844, doi:10.1038/s41586-020-2527-y (2020).
949 39 Daneman, R., Zhou, L., Kebede, A. A. & Barres, B. A. Pericytes are required for blood–
950 brain barrier integrity during embryogenesis. *Nature* **468**, 562-566 (2010).
951 40 Spadoni, I. *et al.* A gut-vascular barrier controls the systemic dissemination of
952 bacteria. *Science* **350**, 830-834, doi:10.1126/science.aad0135 (2015).
953 41 Zhang, X. & van den Pol, A. N. Hypothalamic arcuate nucleus tyrosine hydroxylase
954 neurons play orexigenic role in energy homeostasis. *Nature neuroscience* **19**, 1341-
955 1347 (2016).
956 42 Chen, Q. *et al.* Resident macrophages restrain pathological adipose tissue
957 remodeling and protect vascular integrity in obese mice. *EMBO Rep* **22**, e52835,
958 doi:10.15252/embr.202152835 (2021).
959 43 Almaca, J., Weitz, J., Rodriguez-Diaz, R., Pereira, E. & Caicedo, A. The Pericyte of the
960 Pancreatic Islet Regulates Capillary Diameter and Local Blood Flow. *Cell Metab* **27**,
961 630-644 e634, doi:10.1016/j.cmet.2018.02.016 (2018).
962 44 Loh, K., Herzog, H. & Shi, Y. C. Regulation of energy homeostasis by the NPY system.
963 *Trends Endocrinol Metab* **26**, 125-135, doi:10.1016/j.tem.2015.01.003 (2015).
964 45 Wee, N. K. Y. *et al.* Skeletal phenotype of the neuropeptide Y knockout mouse.
965 *Neuropeptides* **73**, 78-88, doi:10.1016/j.npep.2018.11.009 (2019).
966 46 Mina, A. I. *et al.* CalR: a web-based analysis tool for indirect calorimetry experiments.
967 *Cell metabolism* **28**, 656-666. e651 (2018).
968 47 Renier, N. *et al.* iDISCO: a simple, rapid method to immunolabel large tissue samples
969 for volume imaging. *Cell* **159**, 896-910 (2014).
970 48 Schindelin, J. *et al.* Fiji: an open-source platform for biological-image analysis. *Nature*
971 *methods* **9**, 676-682 (2012).
972 49 Diaz Marin, R., Crespo-Garcia, S., Wilson, A. M. & Sapieha, P. RELi protocol:
973 Optimization for protein extraction from white, brown and beige adipose tissues.
974 *MethodsX* **6**, 918-928, doi:10.1016/j.mex.2019.04.010 (2019).
975 50 Tang, L. *et al.* Isolation and characterization of peritoneal microvascular pericytes.
976 *FEBS Open bio* **12**, 784 (2022).
977 51 Hao, Y. *et al.* Integrated analysis of multimodal single-cell data. *Cell* **184**, 3573-3587.
978 e3529 (2021).
979 52 Muhl, L. *et al.* Single-cell analysis uncovers fibroblast heterogeneity and criteria for
980 fibroblast and mural cell identification and discrimination. *Nat Commun* **11**, 3953,
981 doi:10.1038/s41467-020-17740-1 (2020).
982 53 Carr, M. J. *et al.* Mesenchymal Precursor Cells in Adult Nerves Contribute to
983 Mammalian Tissue Repair and Regeneration. *Cell Stem Cell* **24**, 240-256 e249,
984 doi:10.1016/j.stem.2018.10.024 (2019).
985 54 Kalucka, J. *et al.* Single-Cell Transcriptome Atlas of Murine Endothelial Cells. *Cell* **180**,
986 764-779 e720, doi:10.1016/j.cell.2020.01.015 (2020).
987 55 Bolte, S. & Cordelières, F. P. A guided tour into subcellular colocalization analysis in
988 light microscopy. *Journal of microscopy* **224**, 213-232 (2006).

56 Parlee, S. D., Lentz, S. I., Mori, H. & MacDougald, O. A. in *Methods in enzymology* Vol. 537 93-122 (Elsevier, 2014).

Acknowledgement

We thank I.Kalajzic for sharing the Npy$^{flox/flox}$ mice; M.Silveira and M.Roberts for sharing the Npy1r^{Cre}; Rosa26^{tdTomato} mice; T.Hovarth for sharing the NPY-GFP mice; R. Klemm for the 3T3-L1 cell line; V.Vyazovskiy and S.Wilcox for access to thermo-camera and technical assistance; M.Dustin at the Kennedy Institute of Rheumatology for access to light-sheet microscope, especially C.Lagerholm for his technical assistance; the Dunn School of Pathology for confocal microscopy, especially A.Wainman for his technical assistance; K.Zhang for her technical assistance. We thank INFABIC for their assistance with the inverted microscope Axio Observer Z.1, especially M.O.Baratti and A.T.P.Campos for their help. We thank all the members of Domingos Lab for discussions and advice on the project.

Y.Zhu receives scholarship from Shineroad Industry Developments Co. Ltd. L.Yao is supported by China Scholarship Council. J.Chen is supported by National Natural Science Foundation of China (No. 32100821). This research is funded by the Wellcome Trust -Howard Hughs Medical Institute International research scholar award (208576/Z/17/Z), the ERC consolidator award (ERC-2017 COG 771431), and the Pfizer ASPIRE Obesity award.

Contributions

Y.Z designed and performed all experiments with guidance from A.D unless otherwise stated. Y.Z wrote the first draft of the manuscript and A.D. wrote the subsequent versions with Y.Z. L.Y assisted Y.Z and performed experiments shown in Figure 3, Supplementary Figure 2, 8, 9, 10, 11, and 18f-g with guidance from Y.Z and A.D. A.L.G, B.B, and M.R.S conducted experiments shown in Figure 5c, Supplementary Figures 17e-i and 18a-e with guidance from L.V. G.S helped Y.Z conceive this project and provided advice on scRNA-Seq data analysis. A.C acquired light-sheet images at the Francis Crick Institute on samples cleared and stained by Y.Z shown in Supplementary Figure 14a&c and gave technical advice on light-sheet imaging. N.M. helped with the colony management. C.L imaged the first samples cleared and stained by Y.Z (not shown in this manuscript). M.D permitted access to the Kennedy Imaging Facility; K.A permitted access to the Crick Imaging Facility. T.H provided the brains of NPY-GFP mice shown in Supplementary Figure 19. S.K gave intellectual contributions pertaining to beige fat biology, and I.A. conducted the experiment shown in Supplementary Figure 6a-b, 11c-e with guidance from S.K. J.C conducted the experiments shown in Supplementary Figure 20 with guidance from C.Z. L.Z help with histology shown in Supplementary Figure 8a-b.

Competing Interest Declaration

All authors declare no competing interest.

Fig.1

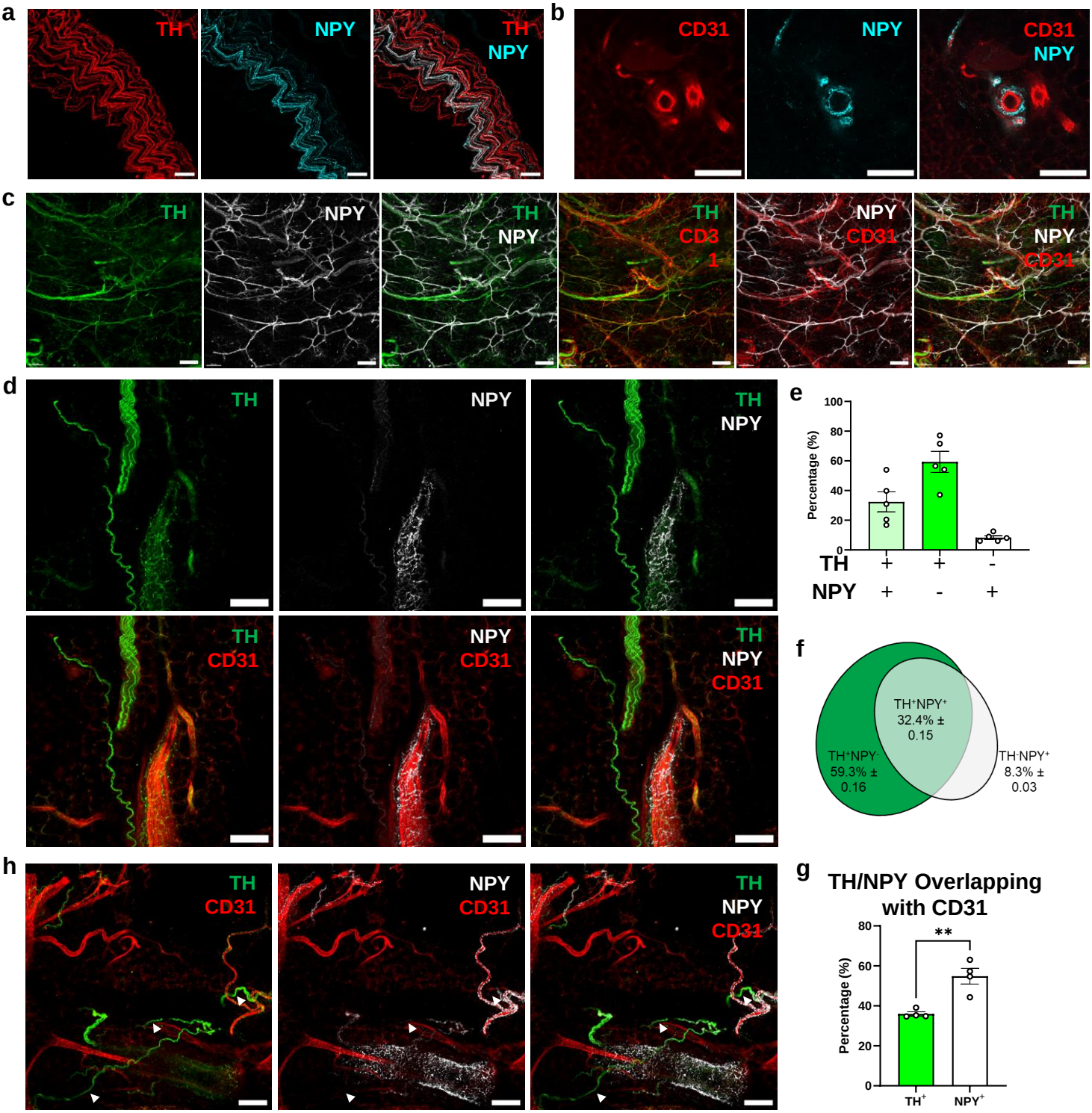
a
TH
NPY
TH
NPY
b
CD31
NPY
CD31
NPY
c
TH
NPY
TH
NPY
TH
CD3
1
NPY
CD31
TH
NPY
CD31
d
TH
NPY
TH
NPY
TH
CD31
NPY
CD31
TH
NPY
CD31
e
Percentage (%)
100
80
60
40
20
0
TH + + -
NPY + - +
f
TH+NPY+
32.4% ±
0.15
TH+NPY-
59.3% ±
0.16
TH-NPY+
8.3% ±
0.03
h
TH
CD31
NPY
CD31
TH
NPY
CD31
g
TH/NPY Overlapping
with CD31
Percentage (%)
80
60
40
20
0
**
TH+
NPY+

Fig.2

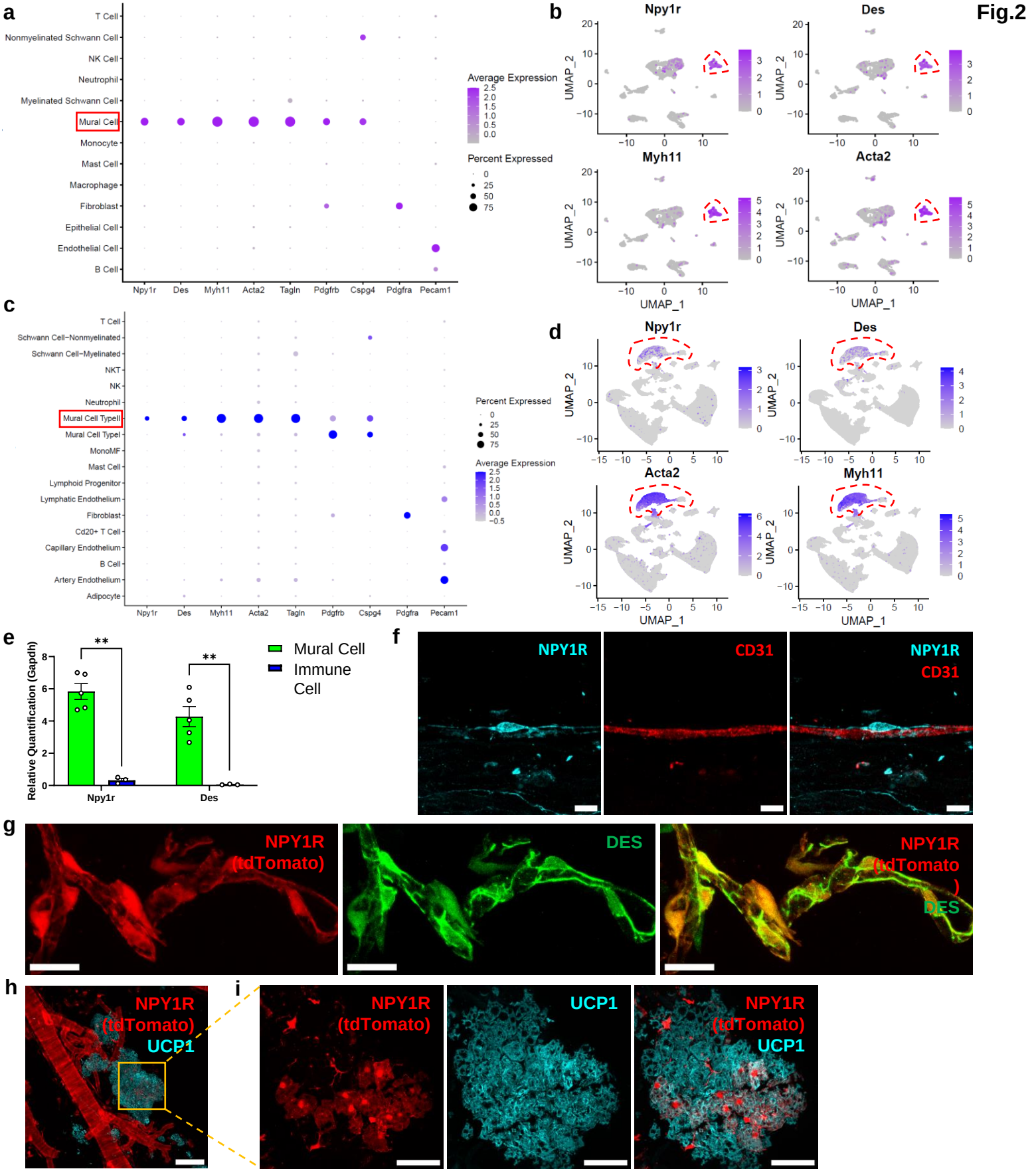
a
T Cell
Nonmyelinated Schwann Cell
NK Cell
Neutrophil
Myelinated Schwann Cell
Mural Cell
Monocyte
Mast Cell
Macrophage
Fibroblast
Epithelial Cell
Endothelial Cell
B Cell
Npy1r
Des
Myh11
Acta2
Tagln
Pdgfrb
Cspg4
Pdgfra
Pecam1
Average Expression
Percent Expressed
b
Npy1r
Des
Myh11
Acta2
UMAP_1
UMAP_2
c
T Cell
Schwann Cell−Nonmyelinated
Schwann Cell−Myelinated
NKT
NK
Neutrophil
Mural Cell TypeII
Mural Cell TypeI
MonoMF
Mast Cell
Lymphoid Progenitor
Lymphatic Endothelium
Fibroblast
Cd20+ T Cell
Capillary Endothelium
B Cell
Artery Endothelium
Adipocyte
d
e
Relative Quantification (Gapdh)
Mural Cell
Immune Cell
f
NPY1R
CD31
g
NPY1R (tdTomato)
DES
h
NPY1R (tdTomato)
UCP1
i

Fig.3

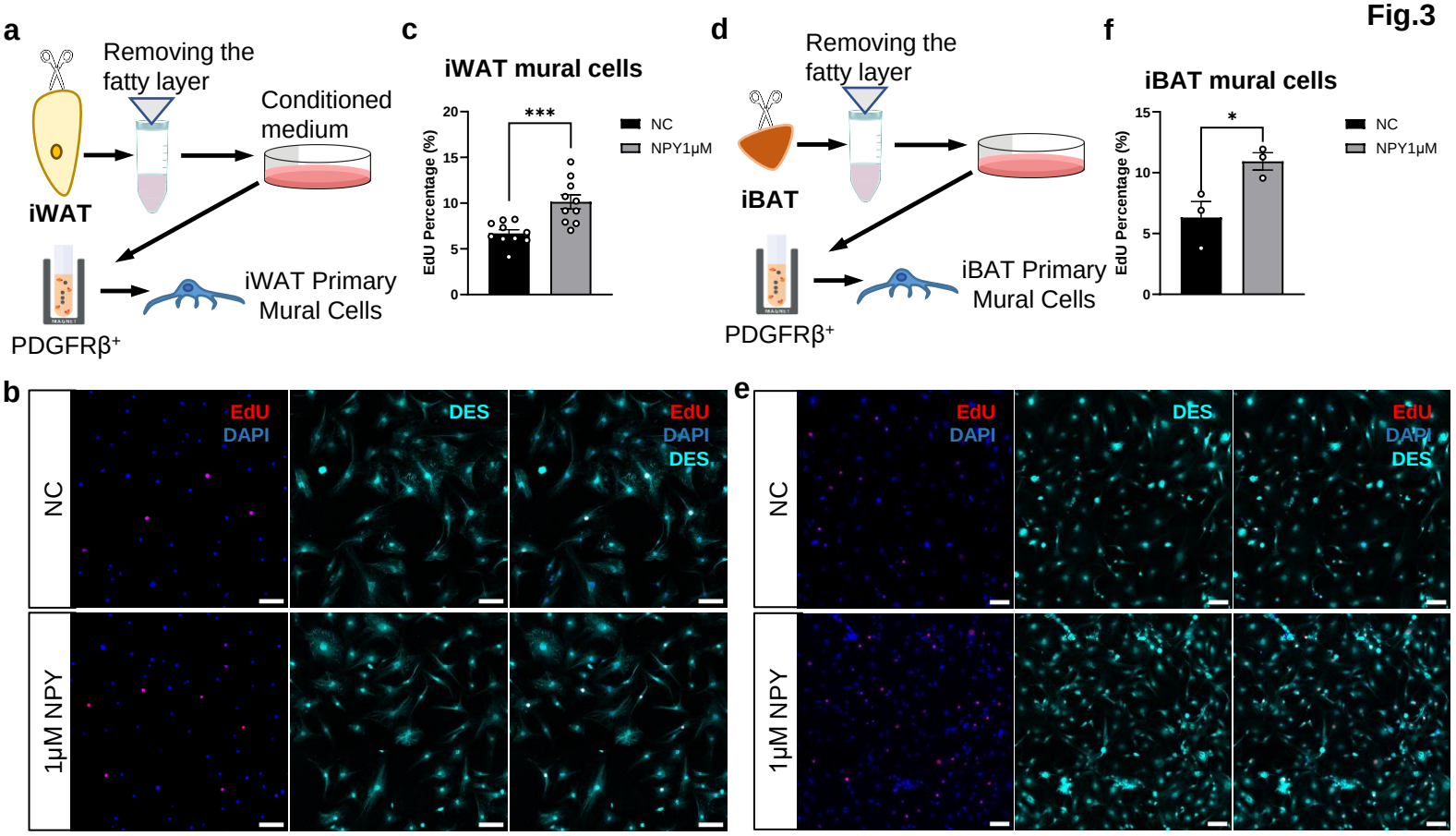
a
Removing the fatty layer
Conditioned medium
iWAT
iWAT Primary Mural Cells
PDGFRβ+
c
iWAT mural cells
EdU Percentage (%)
***
NC
NPY1μM
d
Removing the fatty layer
iBAT
iBAT Primary Mural Cells
PDGFRβ+
f
iBAT mural cells
EdU Percentage (%)
*
NC
NPY1μM
b
NC
1μM NPY
EdU
DAPI
DES
e
NC
1μM NPY
EdU
DAPI
DES

Fig.4

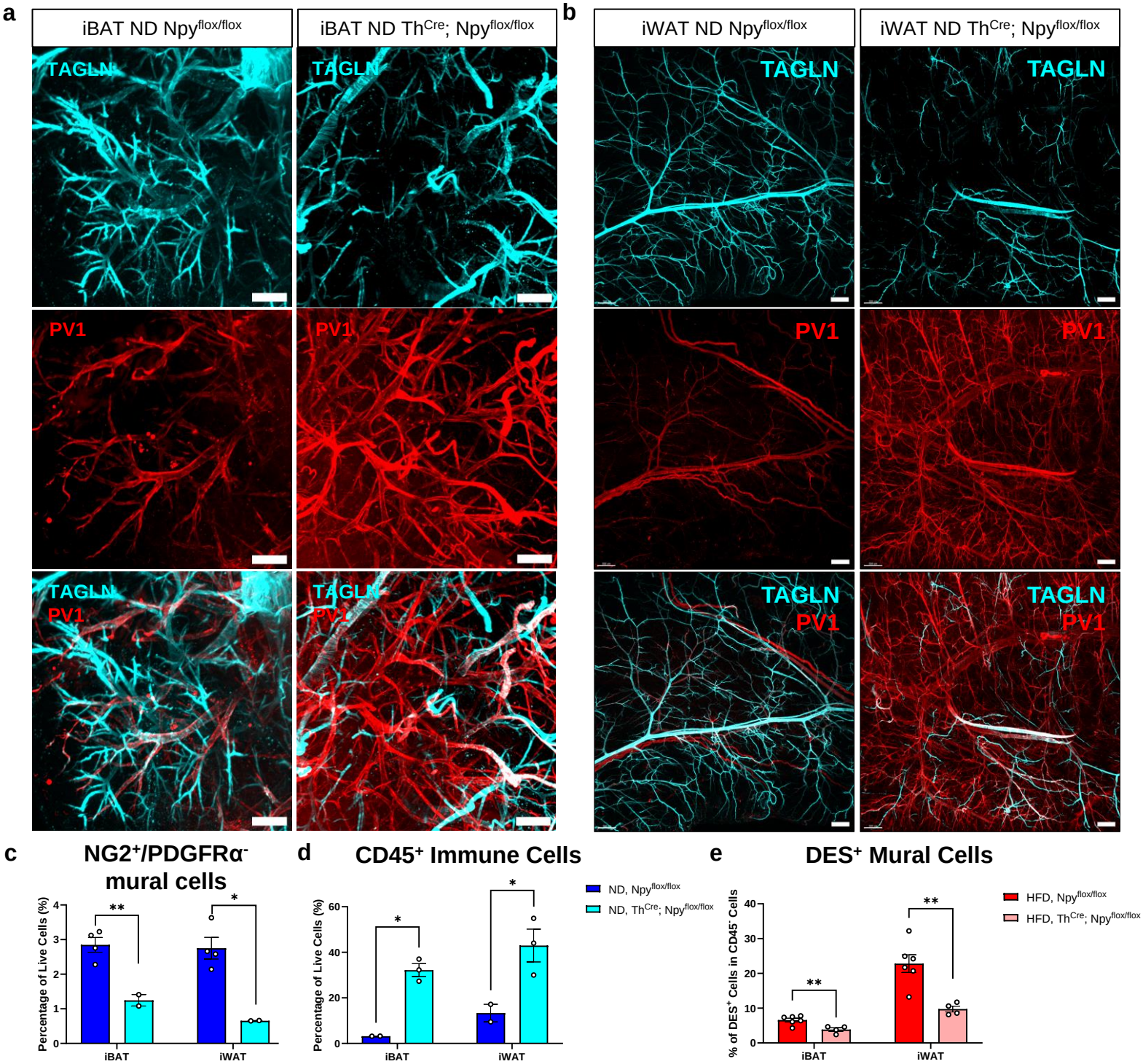
a
iBAT ND Npy flox/flox
iBAT ND Th Cre; Npy flox/flox
b
iWAT ND Npy flox/flox
iWAT ND Th Cre; Npy flox/flox
TAGLN
PV1
TAGLN
PV1
c
NG2+/PDGFRα- mural cells
Percentage of Live Cells (%)
iBAT
iWAT
d
CD45+ Immune Cells
Percentage of Live Cells (%)
ND, Npy flox/flox
ND, Th Cre; Npy flox/flox
e
DES+ Mural Cells
% of DES+ Cells in CD45- Cells
HFD, Npy flox/flox
HFD, Th Cre; Npy flox/flox

Fig.5

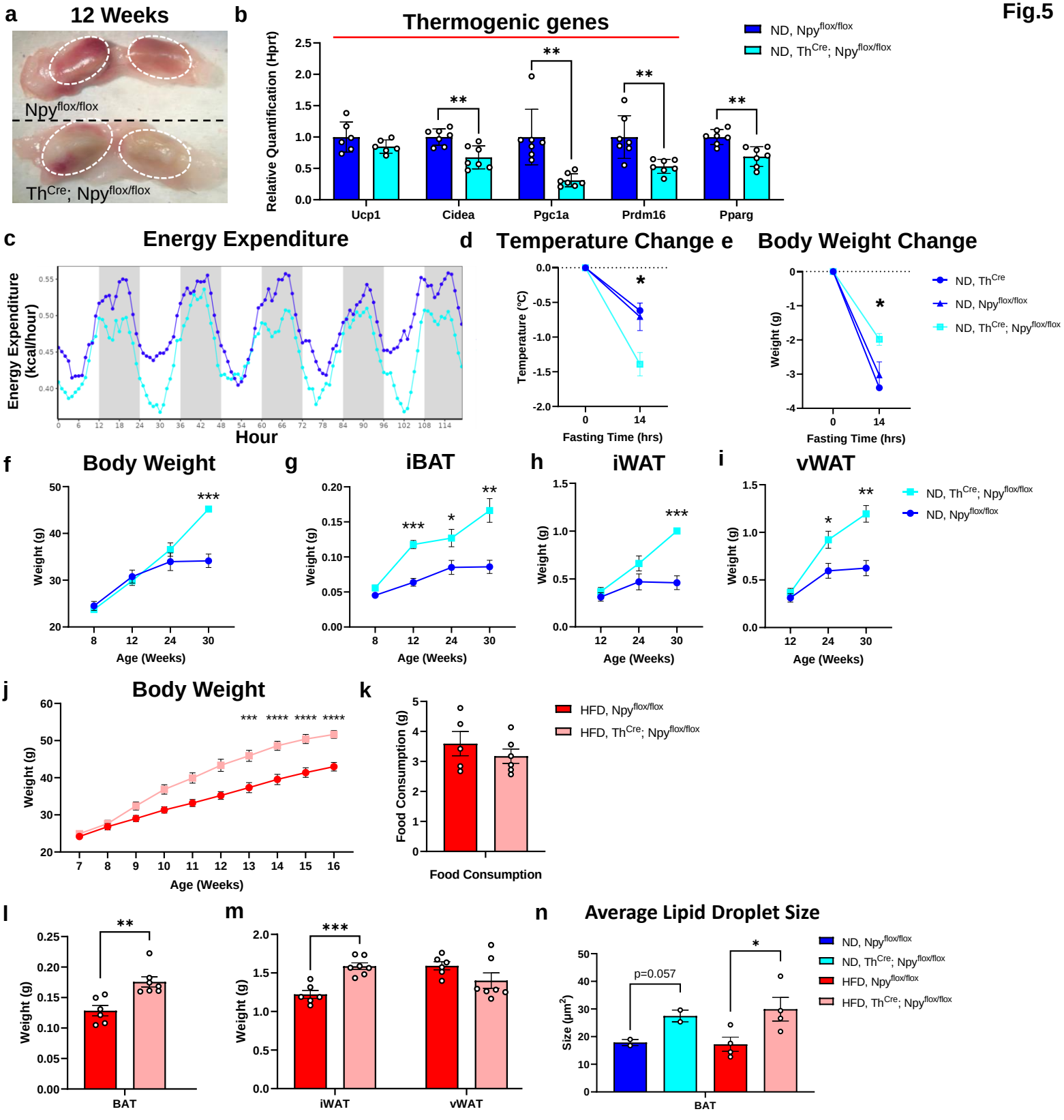
a
12 Weeks
Npy flox/flox
Th Cre; Npy flox/flox
b
Thermogenic genes
Relative Quantification (Hprt)
ND, Npy flox/flox
ND, Th Cre; Npy flox/flox
Ucp1
Cidea
Pgc1a
Prdm16
Pparg
c
Energy Expenditure
Energy Expenditure (kcal/hour)
Hour
d
Temperature Change
Temperature (°C)
Fasting Time (hrs)
e
Body Weight Change
Weight (g)
Fasting Time (hrs)
ND, Th Cre
ND, Npy flox/flox
ND, Th Cre; Npy flox/flox
f
Body Weight
Weight (g)
Age (Weeks)
g
iBAT
Weight (g)
Age (Weeks)
h
iWAT
Weight (g)
Age (Weeks)
i
vWAT
Weight (g)
Age (Weeks)
ND, Th Cre; Npy flox/flox
ND, Npy flox/flox
j
Body Weight
Weight (g)
Age (Weeks)
k
Food Consumption (g)
Food Consumption
HFD, Npy flox/flox
HFD, Th Cre; Npy flox/flox
l
Weight (g)
BAT
m
Weight (g)
iWAT
vWAT
n
Average Lipid Droplet Size
Size (μm²)
p=0.057
BAT
ND, Npy flox/flox
ND, Th Cre; Npy flox/flox
HFD, Npy flox/flox
HFD, Th Cre; Npy flox/flox